


RESEARCH

Open Access



Stimulating effect of graphene oxide on myogenesis of C2C12 myoblasts on RGD peptide-decorated PLGA nanofiber matrices

Yong Cheol Shin¹, Jong Ho Lee¹, Min Jeong Kim¹, Suck Won Hong¹, Bongju Kim², Jung Keun Hyun^{3,4,5}, Yu Suk Choi⁶, Jong-Chul Park^{7*} and Dong-Wook Han^{1*} 

Abstract

Background: In the field of biomedical engineering, many studies have focused on the possible applications of graphene and related nanomaterials due to their potential for use as scaffolds, coating materials and delivery carriers. On the other hand, electrospun nanofiber matrices composed of diverse biocompatible polymers have attracted tremendous attention for tissue engineering and regenerative medicine. However, their combination is intriguing and still challenging.

Results: In the present study, we fabricated nanofiber matrices composed of M13 bacteriophage with RGD peptide displayed on its surface (RGD-M13 phage) and poly(lactic-co-glycolic acid, PLGA) and characterized their physicochemical properties. In addition, the effect of graphene oxide (GO) on the cellular behaviors of C2C12 myoblasts, which were cultured on PLGA decorated with RGD-M13 phage (RGD/PLGA) nanofiber matrices, was investigated. Our results revealed that the RGD/PLGA nanofiber matrices have suitable physicochemical properties as a tissue engineering scaffold and the growth of C2C12 myoblasts were significantly enhanced on the matrices. Moreover, the myogenic differentiation of C2C12 myoblasts was substantially stimulated when they were cultured on the RGD/PLGA matrices in the presence of GO.

Conclusion: In conclusion, these findings propose that the combination of RGD/PLGA nanofiber matrices and GO can be used as a promising strategy for skeletal tissue engineering and regeneration.

Keywords: Graphene oxide, RGD peptide, Poly(lactic-co-glycolic acid), Nanofiber matrix, Myogenic differentiation

Background

The extracellular matrix (ECM) is a network structure composed of various biomolecules, such as collagen, elastin, fibrous protein and cell adhesion protein. The ECM controls the cellular behaviors and provides a favorable microenvironment for the growth of cells [1–3]. In recent years, there have been vigorous efforts to develop three-dimensional scaffolds with not only a suitable structure, but also biofunction for supporting

cellular behaviors [4–6]. The three-dimensional scaffolds can be fabricated using various techniques such as air-spinning, phase separation, emulsion templating, and salt leaching [7, 8]. Among the techniques, electrospinning is an effective and suitable technique for fabricating three-dimensional scaffolds because electrospun matrices have similar structure to the natural ECM, large surface area-to-volume ratio and high porosity [8]. Consequently, electrospun matrices composed of various biomaterials, such as collagen, polyurethane, poly(hydroxybutyrate), and poly(lactic-co-glycolic acid, PLGA), have been applied as tissue engineering scaffolds [9, 10]. Among the various biomaterials used for tissue engineering scaffolds, RGD peptide is one of the most well-known peptides for enhancing the cellular behaviors [11, 12]. The RGD peptide is a tripeptide

* Correspondence: parkjc@yuhs.ac; nanohan@pusan.ac.kr

⁷Cellbiocontrol Laboratory, Department of Medical Engineering, Yonsei University College of Medicine, 50-1, Yonsei-ro, Seodaemun-gu, Seoul 120-752, Korea

¹Department of Optics and Mechatronics Engineering, BK21+ Nano-Integrated Cogno-Mechatronics Engineering, College of Nanoscience & Nanotechnology, Pusan National University, Busandaehak-ro 63beon-gil, Geumjeong-gu, Busan 609-735, >Korea

Full list of author information is available at the end of the article

(Arg-Gly-Asp) found on ECM proteins and a major recognition sequence for integrin that plays an important role in cell adhesion. Therefore, RGD peptide-functionalized substrates can enhance the cellular behavior. In particular, RGD peptide-conjugated substrates based on various biocompatible polymers, such as chitosan, polycaprolactone, poly (L -lactide), polystyrene, and PLGA, have been developed as tissue engineering scaffolds [13–16].

Graphene, a single layer of the sp^2 carbon network with a honeycomb-lattice structure, and its derivatives are considered attractive candidates for biomedical applications including biosensors, scaffolds for tissue engineering, and substrates for the differentiation of stem cells [17–20]. In particular, previous reports have shown that graphene oxide (GO) is non-cytotoxic and has the ability to stimulate the differentiation of myoblasts [21–23]. Therefore, GO can be used to stimulate and promote myogenic differentiation for skeletal tissue regeneration.

Until now, electrospun matrices composed of a wide variety of biodegradable copolymers have been extensively developed for tissue engineering and regeneration as well as drug and gene delivery [9, 24, 25]; however, their use in combination with GO is novel. In the present study, nanofiber matrices composed of PLGA and M13 bacteriophage with RGD peptide displayed on its surface (RGD-M13 phage) were prepared via electrospinning. PLGA is a biodegradable polymer with good cell compatibility that is widely used for the fabrication of tissue engineering scaffolds [26–28]. The M13 phage is a bacterial virus with a long-rod structure [29]. The M13 phage does not have harmful effects on mammalian and human cells [30]. On the other hand, the surface of M13 phage is covered by 2700 major coat proteins (pVIII) that can be modified to express many desired peptides through genetic engineering [31, 32]. In addition, it is conveniently produced by infecting bacterial cell and mass amplification process [33]. Therefore, RGD peptide decoration by using M13 phage is very efficient. The PLGA decorated with RGD-M13 phage (RGD/PLGA) nanofiber matrices were characterized by atomic force microscopy (AFM), Fourier-transform infrared (FTIR) spectroscopy, Raman spectroscopy and thermogravimetric analysis (TGA). Moreover, the cellular behaviors of C2C12 mouse myoblasts on the RGD/PLGA nanofiber matrices were evaluated when GO was added in the culture media to determine if a combination of GO and matrices can be applied as a novel strategy for skeletal tissue regeneration.

Results and discussion

Characterizations of RGD/PLGA nanofiber matrices

The PLGA and RGD/PLGA nanofiber matrices were fabricated by electrospinning and are shown in Fig. 1a

and b. They had a continuous and three-dimensional network structure with interconnected pores that were similar to the natural ECM. The average diameters of the PLGA and RGD/PLGA electrospun fibers were 1440 ± 150 and 200 ± 30 nm, respectively. The diameter of the fabricated nanofibers decreased when RGD-M13 phages were blended (Fig. 1a and b). It was reported that the diameter of the electrospun nanofibers was dependent on the properties of the electrospinning solution, such as viscosity, electrical conductivity, chemical composition, and molecular weight of the constituent polymers [34–36]. When RGD-M13 phage suspension was blended with PLGA, the electrical conductivity of the electrospinning solution was increased due to the salts of the RGD-M13 phage suspension. In addition, the viscosity of the electrospinning solution decreased with the blending of the RGD-M13 phage suspension. Therefore, the diameter of the RGD/PLGA nanofiber decreased compared to that of the PLGA fiber [34]. A decrease in the diameter of the RGD/PLGA nanofibers leads to a significant increase in the surface area-to-volume ratio of the matrices, which in turn leads to an enhanced interaction between the cells and RGD/PLGA matrices [37–39]. Immunofluorescence staining of the RGD-M13 phage was conducted to confirm the presence of the RGD-M13 phage in the hybrid nanofibers. As shown in Fig. 1c, the green fluorescence of the RGD-M13 phages was detected along the RGD/PLGA nanofibers. On the other hand, no fluorescence was detected in the PLGA fiber. It was revealed that the RGD-M13 phages were distributed along the RGD/PLGA nanofibers.

FTIR and Raman spectroscopy were conducted to analyze the composition of the matrices. Figure 2a shows the FTIR spectra of the PLGA matrices, RGD-M13 phages and RGD/PLGA matrices. The typical bands of PLGA were observed at 1750 and 1080 cm^{-1} , which represented the C=O stretching and C-O stretching modes of the ester group, respectively [40]. Additionally, another band was observed at 1180 cm^{-1} , which was assigned to the C-O-C stretching [41]. On the other hand, in the RGD/PLGA matrices, the characteristic bands of RGD-M13 phage were found near 1630 , 1450 and 1280 cm^{-1} , which can be attributed to the amide I, II and III vibrations from protein structure, respectively [42, 43]. This result was well supported by Raman spectrum of RGD/PLGA matrices which showed the characteristic peaks of RGD-M13 phages. As shown in the Fig. 2b, the peaks for the RGD-M13 phages were apparently observed near 1200 , 1560 and 1660 cm^{-1} , which can be assigned to the NH_3^+ , amide II and amide I groups, respectively [44–46]. The thermal stability of the matrices was evaluated by TGA (Fig. 2c). The onset of the decomposition temperatures of the PLGA and RGD/

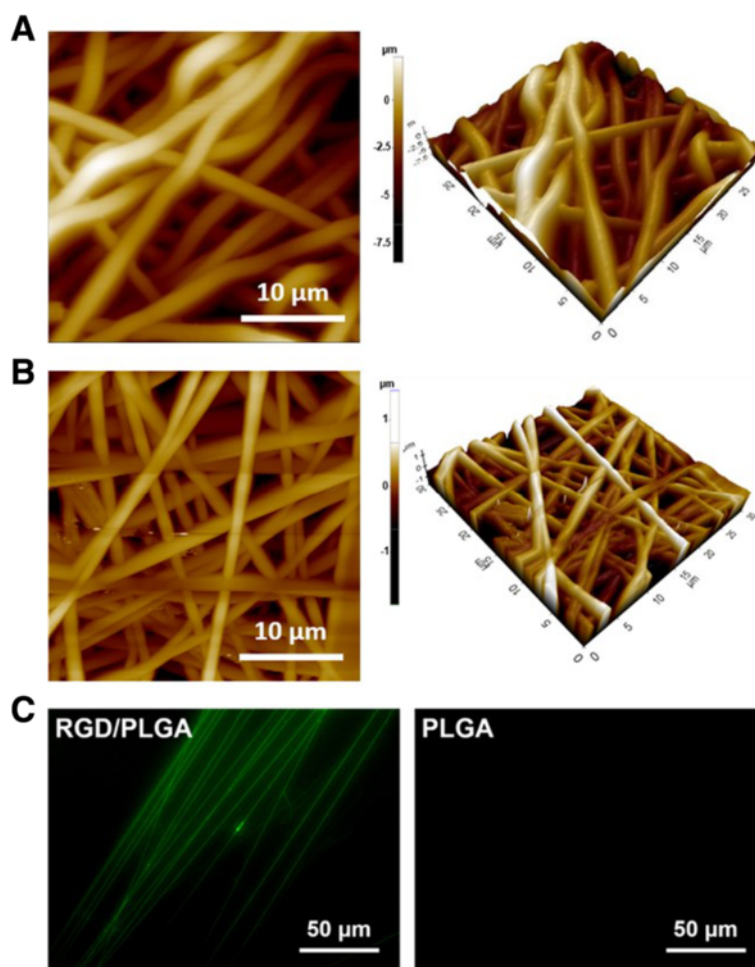


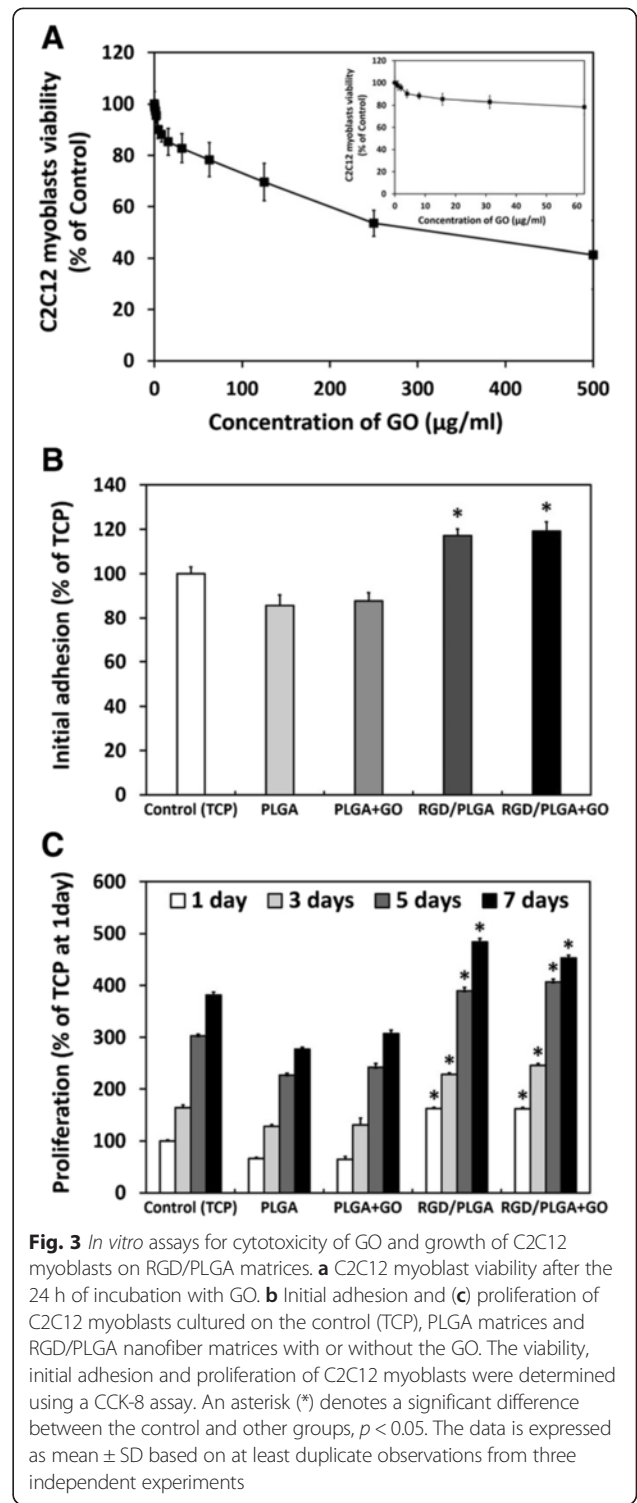
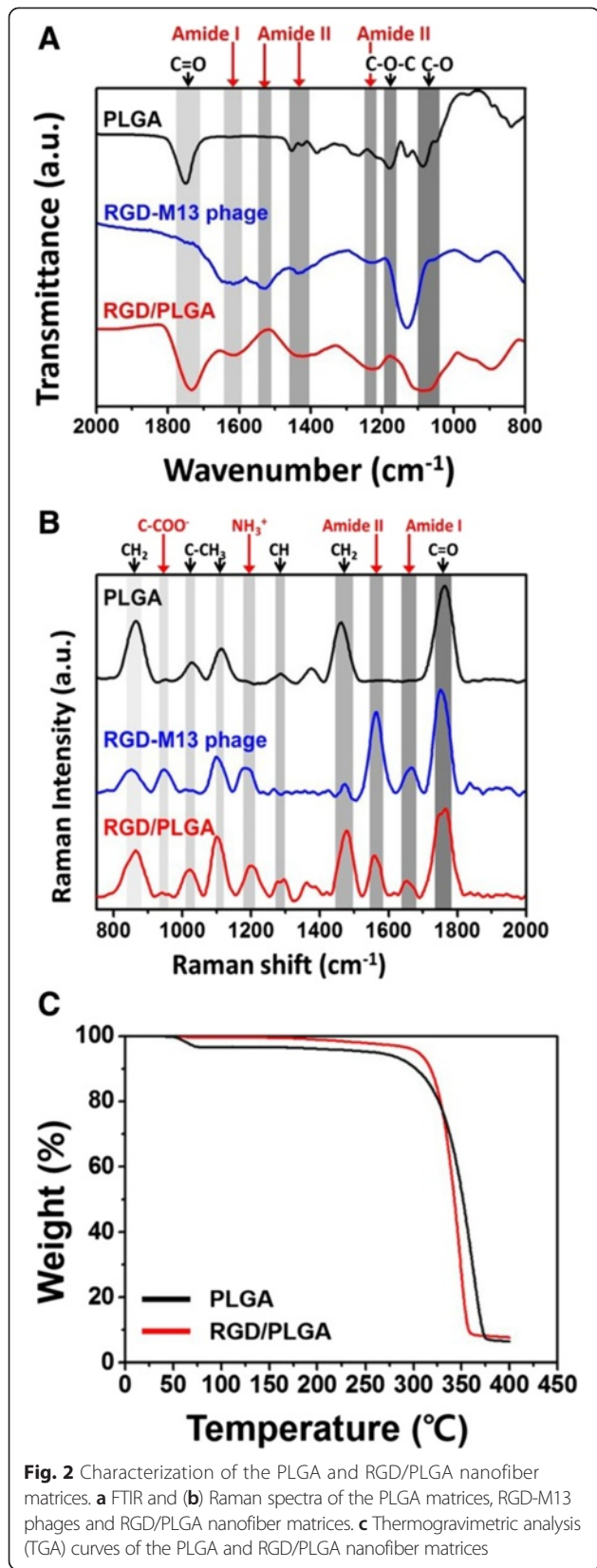
Fig. 1 Surface morphology and immunostaining of electrospun nanofibers. AFM images of (a) PLGA and (b) RGD/PLGA nanofiber matrices. c Immunofluorescence images of PLGA and RGD/PLGA electrospun fibers. RGD peptide-displaying M13 phages in the RGD/PLGA nanofibers were immunostained with the FITC-labeled anti-M13 phage antibody (green). All photographs shown in this figure are representative of six independent experiments with similar results

PLGA nanofiber matrices were approximately 280 and 300 °C, respectively. No significant difference was observed between the two types of matrices. The results from the FTIR spectra and TGA revealed that the RGD/PLGA nanofibers were successfully fabricated and the RGD-M13 phages were evenly distributed throughout the matrices. Moreover, the addition of RGD-M13 phage did not adversely affect the thermal stability of the matrices, and the matrices were thermally stable under cell culture conditions. Therefore, it is suggested that the RGD/PLGA nanofiber matrices have a suitable structure and physicochemical properties as a cellular scaffold.

Cytotoxicity of GO and growth of C2C12 myoblasts on RGD/PLGA nanofiber matrices

The influence of GO on the growth of cells is highly dependent on its size, shape and concentration [47–49]. Therefore, to evaluate the cell compatibility of the GO

and RGD/PLGA matrices, *in vitro* assays for cytotoxicity of GO and growth of C2C12 myoblasts on RGD/PLGA nanofiber matrices with 10 μg/ml of GO were conducted using a cell counting kit-8 (CCK-8) assay, based on the mitochondrial activity (Fig. 3). As shown in Fig. 3a, the viability of the C2C12 myoblasts decreased with increasing GO concentration. The cell viability was slightly ($p < 0.05$) decreased at concentrations lower than 62.5 μg/ml, whereas it was significantly ($p < 0.05$) decreased at higher concentrations (≥ 100 μg/ml). The C2C12 myoblasts viability decreased to approximately 40 % of the control at 500 μg/ml GO. According to previous literature, the cytotoxicity of GO involves the oxidative stress response [48]. GO has been reported to exhibit dose-dependent cytotoxicity but did not show apparent cytotoxicity at a low concentration [21, 48, 49]. Our results are in accordance with previous studies. In the present study, GO was cytotoxic to C2C12 myoblasts at

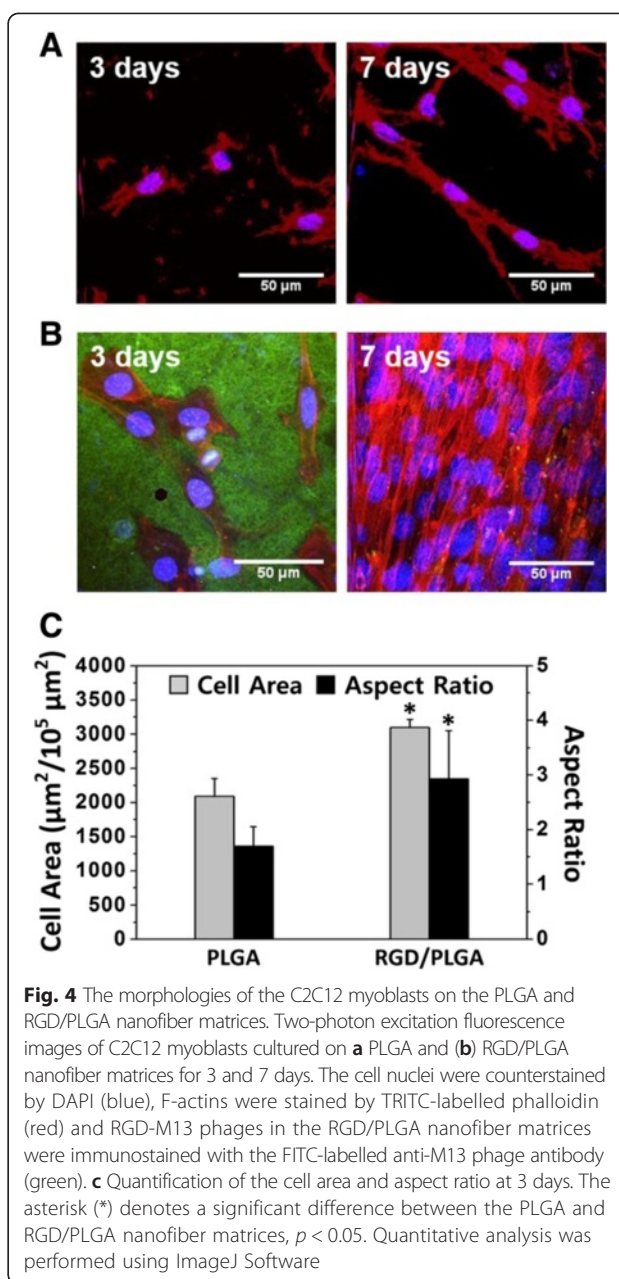


high concentrations ($\geq 100 \mu\text{g/ml}$) but not at low concentrations ($< 62.5 \mu\text{g/ml}$) (Fig. 3a). These results indicated that the GO has no harmful effects on C2C12 myoblasts and is non-cytotoxic at $10 \mu\text{g/ml}$.

The initial adhesion and proliferation of C2C12 myoblasts on the tissue culture plastics (TCPs), PLGA

matrices, and RGD/PLGA nanofiber matrices were also evaluated. In addition, C2C12 myoblasts on the PLGA and RGD/PLGA matrices were incubated in the culture media containing 10 $\mu\text{g/ml}$ of GO to examine the effects of GO. The initial adhesion of C2C12 myoblasts was significantly ($p < 0.05$) promoted on the RGD/PLGA matrices compared to that on the TCPs and PLGA matrices, regardless of the addition of GO (Fig. 3b). Moreover, as shown in Fig. 3c, the proliferation of C2C12 myoblasts was significantly ($p < 0.05$) increased on the RGD/PLGA matrices, while it was slightly done in the GO-added groups. RGD peptide-conjugated substrates were reported to enhance not only cell adhesion, but also proliferation [13–16]. In addition, these enhanced initial adhesion and proliferation might be also due to the fact that the increased surface area-to-volume ratio can facilitate the interaction between cells and matrices. On the other hand, the proliferation of C2C12 myoblasts was highest when they were cultured on the RGD/PLGA matrices supplemented with GO for 5 days of culture. According to previous reports, GO can also support cellular behaviors, including cell adhesion and proliferation [18, 19, 50]. At 7 days after culture, however, the increase in proliferation rate was reduced. This might be due to the fact that C2C12 myoblasts were sufficiently grown and began to differentiate into myotubes rather than proliferate [51, 52].

Figure 4 shows the morphologies of the C2C12 myoblasts on the PLGA and RGD/PLGA matrices for 3 and 7 days. As shown in Fig. 4a, the C2C12 myoblasts on the PLGA matrices were unable to form F-actin properly and the number of cells did not appreciably increase. On the other hand, the C2C12 myoblasts on the RGD/PLGA matrices showed a spindle-like morphology with well-organized F-actins and the number of cells was significantly increased (Fig. 4b). This can be explained by the fact that the RGD peptide moieties, which exist on the RGD/PLGA matrices, stimulate cell adhesion, and promote the proliferation of cells. Additionally, the green fluorescence of the RGD-M13 phages was observed throughout the RGD/PLGA nanofibers. These stimulated adhesion and proliferation of myoblasts were also demonstrated by quantitative analysis of the cell morphology (Fig. 4c). The cell area of the C2C12 myoblasts on the RGD/PLGA matrices were significantly ($p < 0.05$) increased by enhancing the adhesion (Fig. 4c). In addition, the aspect ratio of C2C12 myoblasts on the RGD/PLGA matrices was increased. Generally, the cellular extension of C2C12 myoblasts was favorable for the fusion of the neighboring cells and was considered to be the initiation of myogenic differentiation [23, 53, 54]. These results indicated that the RGD/PLGA nanofiber matrices effectively support the growth and differentiation of C2C12 myoblasts.



Myogenic differentiation of C2C12 myoblasts on RGD/PLGA nanofiber matrices

The myogenic differentiation of C2C12 myoblasts was evaluated by immunofluorescence staining for myosin heavy chain (MHC). MHC is a well-characterized marker for the myogenic differentiation of skeletal muscle cells [55]. The C2C12 myoblasts were cultured on the PLGA or RGD/PLGA matrices and incubated in growth media (GM) containing 10 $\mu\text{g/ml}$ of GO for 5 days. As shown in Fig. 5a, the C2C12 myoblasts on PLGA matrices showed an unusual morphology with poorly-developed F-actin network and cellular debris. In addition, they did not differentiate because the number of cells was insufficient to

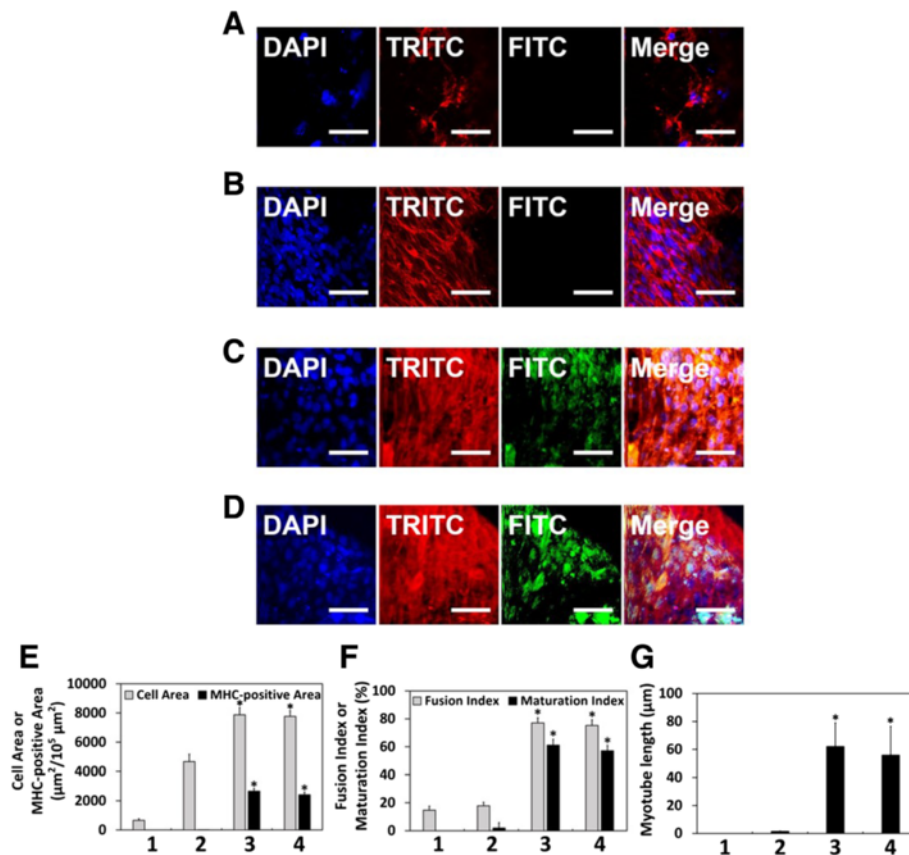


Fig. 5 Stimulated myogenesis of C2C12 myoblasts on RGD/PLGA nanofiber matrices. Two-photon excitation fluorescence images of the C2C12 myoblasts on (a) PLGA and (b) RGD/PLGA nanofiber matrices without the GO, (c) RGD/PLGA nanofiber matrices with the GO and (d) RGD/PLGA nanofiber matrices in differentiation media (DM). The cell nuclei were counterstained by DAPI (blue), F-actins were stained with TRITC-labelled phalloidin (red) and the myosin heavy chains (MHCs) were stained with FITC-labelled anti-MHC antibody (green). The scale bars are 50 μm . All photographs shown in this figure are representative of six independent experiments with similar results. Quantification of (e) the cell area, MHC-positive area, (f) fusion index, maturation index, and (g) myotube length (1: PLGA matrices, 2: RGD/PLGA nanofiber matrices without the GO, 3: RGD/PLGA nanofiber matrices with the GO, and 4: RGD/PLGA nanofiber matrices in DM). An asterisk (*) denotes a significant difference between PLGA matrices and other groups, $p < 0.05$. Quantitative analysis was performed using ImageJ Software

differentiate. It is known that the C2C12 myoblasts can be differentiated when they are fully proliferated in differentiation media (DM) [56, 57]. Therefore, the C2C12 myoblasts on the PLGA matrices could not be differentiated and the green fluorescence of MHC was not exhibited. The C2C12 myoblasts cultured on the RGD/PLGA matrices without the GO were well-grown but did not differentiate into mature myotubes, which is evidence of myogenic differentiation (Fig. 5b). On the RGD/PLGA matrices with the GO, however, the C2C12 myoblasts were fully proliferated and differentiated with multinucleate myotubes (Fig. 5c). In addition, the green fluorescence of MHC was observed from the myotubes. On the other hand, the C2C12 myoblasts cultured on the RGD/PLGA matrices in DM were differentiated as a positive control (Fig. 5d). This was also supported by quantification of the MHC-positive area, fusion index, maturation index, and myotube length. As shown in

Fig. 5e, the cell area and MHC-positive area of the C2C12 myoblasts cultured on the RGD/PLGA matrices in the presence of the GO were significantly ($p < 0.05$) higher than those on PLGA and RGD/PLGA matrices in the absence the GO. No difference in cell area and MHC-positive area was observed between the GO-added groups and positive controls (cultured on RGD/PLGA matrices in DM). We also quantified the myogenic differentiation of C2C12 myoblasts by analyzing the fusion index, maturation index and myotube length. As shown in Fig. 5f and g, the fusion index, maturation index and myotube length significantly ($p < 0.05$) increased when the C2C12 myoblasts were cultured on the RGD/PLGA matrices in combination with GO or in DM. Consequently, it was revealed that the differentiation of the C2C12 myoblasts was effectively stimulated by the synergistic effect of the RGD/PLGA matrices and GO. The RGD/PLGA matrices promoted cell proliferation and

GO stimulated cell differentiation. According to previous studies, the enhancement of cell adhesion and proliferation accelerates the differentiation of the C2C12 myoblasts [58–61]. In addition, many studies showed that GO can stimulate the differentiation of various types of cells as well as myoblasts [19, 20, 23, 62, 63]. Therefore, it is suggested that the RGD/PLGA matrices are suitable scaffolds for the growth of C2C12 myoblasts. Furthermore, their use in combination with GO can stimulate and accelerate the myogenic differentiation of C2C12 myoblasts.

Conclusions

This study developed biofunctional scaffolds that can promote the proliferation and differentiation of C2C12 myoblasts. The RGD/PLGA nanofiber matrices were successfully fabricated by electrospinning and the characteristics of the matrices were investigated. Our results showed that the structure of the RGD/PLGA nanofiber matrices was dimensionally similar to that of the natural ECM and the RGD-M13 phages were homogeneously distributed in the matrices. It was confirmed that the RGD/PLGA matrices were cell compatible and could support the growth and proliferation of C2C12 myoblasts. In addition, when the matrices were used with GO, the myogenic differentiation of C2C12 myoblasts was effectively stimulated and accelerated. In conclusion, it is suggested that the RGD/PLGA nanofiber matrices are suitable scaffolds with the ability to support cellular behaviors. Moreover, the matrices can be used in combination with GO as a novel strategy for skeletal tissue regeneration and treatment of muscle dysfunction by stimulating the differentiation of myoblasts. Further studies with GO-loaded RGD/PLGA nanofiber matrices are needed to employ the approach presented in this study for *in vivo* applications.

Methods

Preparation of RGD/PLGA nanofiber matrices

RGD peptides were displayed on major coat protein that wraps the side wall of the M13 phage cloning method according to previously described procedure [31, 32]. Briefly, to incorporate the RGD peptide sequences, polymerase chain reaction was carried out using Phusion DNA Polymerase, two primers and an M13KE vector [64]. The engineered M13KE phages were amplified in bacterial cells and concentrated by polyethylene glycol precipitation.

The RGD/PLGA nanofiber matrices were prepared by electrospinning. Briefly, PLGA resins [PLA/PGLA = 75/25, molecular weight = 70–110 kDa, Evonik Industries, Essen, Germany] were dissolved in 1, 1, 1, 3, 3, 3-hexafluoroisopropanol (HFIP, Sigma-Aldrich Co., St Louis, MO) at a concentration of 200 mg/ml. The RGD-

M13 phage suspensions in tris buffered saline (TBS) buffer (50 mM tris and 150 mM NaCl, pH 7.4, Bioworld, Dublin, OH) were blended with the PLGA solution. The concentration of RGD-M13 phages was 10 mg/ml. The mixture solution of PLGA and RGD-M13 phages was loaded into a syringe fitted with a 25 G needle. A voltage of 14 kV was applied and the working distance between the needle tip and the collector was 11 cm. The flow rate of the mixture solution was 0.2 ml/h. Randomly-oriented RGD/PLGA nanofibers were collected on a steel rotating wheel covered with aluminum foil. The RGD/PLGA nanofiber matrices were then dried overnight under vacuum at room temperature (RT) to remove any residual solvent.

Characterizations of RGD/PLGA nanofiber matrices

The surface morphology of the RGD/PLGA nanofiber matrices was observed by AFM (NX10, Park Systems Co., Suwon, Korea) with a Multi 75 silicon scanning probe. Immunofluorescence staining for RGD-M13 phages was conducted to examine the existence of RGD-M13 phages in the RGD/PLGA nanofibers. The RGD/PLGA nanofibers were incubated with the primary anti-M13 phage antibody for 2 h at RT and then incubated with secondary fluorescein isothiocyanate (FITC)-conjugated goat anti-rabbit IgG for 1 h at RT. The immunostained nanofibers were imaged with an Olympus IX81 inverted fluorescence microscope. The composition of the PLGA, RGD-M13 phage, and RGD/PLGA nanofiber matrices was characterized by FTIR and Raman spectroscopy. The FTIR spectra were collected using a FTIR spectrophotometer (Nicolet 560, Nicolet Co., Madison, WI). All spectra were recorded in absorption mode in the wavelength range of 800–2000 cm^{-1} with a resolution of 4.0 cm^{-1} and 16-times scanning. The Raman spectra were obtained by a Raman spectroscope (Micro Raman PL Mapping System, Dongwoo Optron Co., Ltd, Gwangju-si, Korea) with an Ar-ion laser of wavelength 514.5 nm at a power of 5 mW. The FTIR and Raman spectra were baselined to minimize the effect of the background (slope) by using ORIGIN 8.0[®] program (OriginLab Corporation, Northampton, MA). The thermal stability of the PLGA and RGD/PLGA nanofiber matrices was evaluated by TGA (TGA n-1000, Scinco Co., Seoul, Korea). Samples were weighed (approximately 5 mg) in open aluminum pans and heated from 25 to 400 °C at a heating rate of 10 °C/min.

Cytotoxicity of GO and growth of C2C12 myoblasts

The C2C12 mouse myoblasts were purchased from the American Type Culture Collection (Rockville, MD) and routinely maintained in GM, Dulbecco's modified Eagle's Medium (DMEM, Welgene, Daegu, Korea) supplemented with 10 % fetal bovine serum (FBS, Welgene) and a 1 % antibiotic-antimycotic solution (containing

10,000 units penicillin, 10 mg streptomycin and 25 μg amphotericin B per ml, Sigma-Aldrich Co.) at 37 °C in a humidified atmosphere containing 5 % CO_2 .

GO was prepared from expanded graphite according to the modified Hummers and Offeman method as described in our previous work [65, 66]. The cytotoxicity of GO for the C2C12 myoblasts was assessed using a CCK-8 assay (Dojindo, Kumamoto, Japan) according to the manufacturer's instructions. The number of viable cells was found to be directly proportional to the metabolic reaction products obtained in the CCK-8 assay [24, 67]. Briefly, the C2C12 myoblasts were seeded at a density of 5×10^4 cells/ml on 24-well plates in 1 ml of GM and incubated for 24 h. Subsequently, GO was added with increasing concentrations (0 to 500 $\mu\text{g}/\text{ml}$) to the culture media and the cells were incubated with a CCK-8 solution for the last 2 h of the culture period (24 h) at 37 °C in the dark. The absorbance was measured at 450 nm using an ELISA reader (SpectraMax 340, Molecular Device Co., Sunnyvale, CA).

The initial adhesion and proliferation of C2C12 myoblasts was determined by a CCK-8 assay, as described above. The cells were seeded on the PLGA and RGD/PLGA matrices at a density of 1×10^4 cells/ml in 1 ml of GM. To examine the effects of GO, the C2C12 myoblasts on the PLGA and RGD/PLGA matrices were cultured in GM containing 10 $\mu\text{g}/\text{ml}$ of GO. Each cell culture was incubated with a CCK-8 solution for the last 2 h of the culture period for initial adhesion (6 h) and proliferation (1, 3, 5 and 7 days) at 37 °C in the dark. Parallel sets of C2C12 myoblasts were cultured on TCPs and results were regarded as positive (+) controls.

Immunofluorescence staining of C2C12 myoblasts

For the morphological observations, C2C12 myoblasts cultured on the PLGA or RGD/PLGA matrices for 3 and 7 days were fixed with a 3.7 % formaldehyde solution (Sigma-Aldrich Co.) for 10 min. After fixation, the cells were immersed in a 0.1 % Triton X-100 (Sigma-Aldrich Co.) solution for 5 min and then blocked with a 2 % bovine serum albumin (BSA, GenDEPOT, Barker, TX) solution in Dulbecco's phosphate-buffered saline (DPBS, Gibco BRL, Rockville, MD) for 30 min. After blocking, the cells were incubated with TRITC-labeled phalloidin (Molecular Probes, Eugene, OR) for 20 min at RT. The cell nuclei were counterstained with 1 μM of 4',6-diamidino-2-phenylindole (DAPI, Sigma-Aldrich Co.). The C2C12 myoblasts-cultured matrices were immunostained with the primary and secondary antibodies as described in 'Characterizations of RGD/PLGA nanofiber matrices' section of Methods. The fluorescence images were observed using a custom-built two-photon excitation fluorescence microscope, as described elsewhere [68, 69]. The fluorescence images were analyzed

using ImageJ software (National Institutes of Health, Bethesda, MD). Quantitative analysis of the cell morphology was carried out by measuring the cell area and calculating the aspect ratio.

To examine the myogenic differentiation of C2C12 myoblasts, the MHCs were stained with the Alexa Fluor 488 conjugated anti-MHC monoclonal antibody (eBioscience Inc., San Diego, CA). The C2C12 myoblasts were cultured on the PLGA or RGD/PLGA matrices for 24 h. The cells on the matrices were then incubated in GM or DM containing 10 $\mu\text{g}/\text{ml}$ of GO. The fluorescence images were observed after the additional 5 days of incubation. The C2C12 myoblasts were cultured on the RGD/PLGA matrices in DM (low-serum media, DMEM containing 2 % of horse serum and 1 % antibiotic-antimycotic solution) and the results were regarded as positive (+) controls. Quantitative analysis of the myogenic differentiation of C2C12 myoblasts was conducted by analyzing the fusion index, maturation index and myotube length. The fusion index was obtained by calculating the percentage of the number of nuclei within the multinucleate myotubes containing more than two nuclei to the total number of nuclei. The maturation index was calculated as the percentage of myotubes containing more than five nuclei to the total number of myotubes [23].

Statistical analysis

All variables were tested in three independent cultures for each experiment, which was repeated twice ($n = 6$). All the quantitative data is expressed as the mean \pm standard deviation (SD). Statistical comparisons were carried out by a one-way analysis of variance (ANOVA), followed by a Bonferroni test for multiple comparisons. A value of $p < 0.05$ was considered statistically significant.

Abbreviations

AFM: Atomic force microscopy; ANOVA: Analysis of variance; BSA: Bovine serum albumin; CCK-8: Cell counting kit-8; DAPI: 4',6-Diamidino-2-phenylindole; DM: Differentiation media; DMEM: Dulbecco's modified Eagle's Medium; DPBS: Dulbecco's phosphate-buffered saline; ECM: Extracellular matrix; FBS: Fetal bovine serum; FITC: Fluorescein isothiocyanate; FTIR: Fourier-transform infrared; GM: Growth media; GO: Graphene oxide; HFIP: 1, 1, 1, 3, 3, 3-Hexafluoroisopropanol; MHC: Myosin heavy chain; PLGA: Poly(lactic-co-glycolic acid); RGD peptide: Arg-Gly-Asp; RGD/PLGA: PLGA decorated with RGD-M13 phage; RGD-M13 phage: M13 bacteriophage with RGD peptide displayed on its surface; RT: Room temperature; SD: Standard deviation; TBS: Tris buffered saline; TCP: Tissue culture plastic; TGA: Thermogravimetric analysis.

Competing interests

The authors report no conflicts of interest in this work.

Authors' contributions

YCS designed the experiments, fabricated the nanofiber matrices by electrospinning, participated in the acquisition of the immunofluorescence staining images, and drafted the manuscript. JHL and MJK carried out the characterizations of RGD/PLGA nanofiber matrices. SWH prepared the GO and contributed in the cell cultures and *in vitro* assays. JWO performed the genetic engineering of M13 phages. CSK and BK participated in the quantitative

analysis of the two-photon excitation fluorescence images. JKH and YSC performed the statistical analysis and helped interpret the data. DWH conceived of the study, participated in its design and coordination, and helped to draft the manuscript. All authors read and approved the final manuscript.

Acknowledgments

This study was supported by grants of the Korea Health Technology R&D Project through the Korea Health Industry Development Institute, funded by the Ministry of Health & Welfare, Republic of Korea (No. HI14C0522) and of the Bio & Medical Technology Development Program of the National Research Foundation (NRF) funded by the Korean government (MEST) (No. 2015M3A9E2028643).

Author details

¹Department of Optics and Mechatronics Engineering, BK21+ Nano-Integrated Cogno-Mechatronics Engineering, College of Nanoscience & Nanotechnology, Pusan National University, Busandaehak-ro 63beon-gil, Geumjeong-gu, Busan 609-735, >Korea. ²Clinical Dental Research Institute, Seoul National University Dental Hospital, Seoul 03080, Korea. ³Department of Rehabilitation Medicine, College of Medicine, Cheonan 330-714, Korea. ⁴Department of Nanobiomedical Science & BK21+ NBM Global Research Center, Cheonan 330-714, Korea. ⁵Institute of Tissue Regeneration Engineering, Dankook University, Cheonan 330-714, Korea. ⁶School of Anatomy, Physiology, and Human Biology, University of Western Australia, Crawley, WA 6009, Australia. ⁷Cellbioccontrol Laboratory, Department of Medical Engineering, Yonsei University College of Medicine, 50-1, Yonsei-ro, Seodaemun-gu, Seoul 120-752, Korea.

Received: 21 September 2015 Accepted: 17 November 2015

Published online: 25 November 2015

References

- Juliano RL, Haskill S. Signal transduction from the extracellular matrix. *J Cell Biol.* 1993;120(3):577–85.
- Meredith Jr JE, Fazeli B, Schwartz MA. The extracellular matrix as a cell survival factor. *Mol Biol Cell.* 1993;4(9):953–61.
- Théry M, Racine V, Pépin A, Piel M, Chen Y, Sibarita JB, et al. The extracellular matrix guides the orientation of the cell division axis. *Nat Cell Biol.* 2005;7(10):947–53.
- Snyder TN, Madhavan K, Intrator M, Dregalla RC, Park D. A fibrin/hyaluronic acid hydrogel for the delivery of mesenchymal stem cells and potential for articular cartilage repair. *J Biol Eng.* 2014;8:10.
- Kim J, Lin B, Kim S, Choi B, Evseenko D, Lee M. TGF- β 1 conjugated chitosan collagen hydrogels induce chondrogenic differentiation of human synovium-derived stem cells. *J Biol Eng.* 2015;9:1.
- Shin YC, Lee JH, Jin OS, Lee EJ, Jin L, Kim CS, et al. RGD peptide-displaying M13 bacteriophage/PLGA nanofibers as cell-adhesive matrices for smooth muscle cells. *J Korean Phys Soc.* 2015;66(1):12–6.
- Sabbatier G, Larrañaga A, Guay-Bégin AA, Fernandez J, Diéval F, Durand B, et al. Design, degradation mechanism and long-term cytotoxicity of poly(L-lactide) and poly(lactide-co- ϵ -caprolactone) terpolymer film and air-spun nanofiber scaffold. *Macromol Biosci.* 2015;15(10):1392–410.
- Kim MS, Lee MH, Kwon BJ, Koo MA, Seon KM, Park JC. Enhancement of human mesenchymal stem cell infiltration into the electrospun poly(lactide-co-glycolic acid) scaffold by fluid shear stress. *Biochem Biophys Res Commun.* 2015;463:137–42.
- Lee S, Jin G, Jang JH. Electrospun nanofibers as versatile interfaces for efficient gene delivery. *J Biol Eng.* 2014;8:30.
- Shin YC, Lee JH, Kim MJ, Park JH, Kim SE, Kim JS, et al. Biomimetic hybrid nanofiber sheets composed of RGD peptide-decorated PLGA as cell-adhesive substrates. *J Funct Biomater.* 2015;6(2):367–78.
- Pytela R, Pierschbacher MD, Ginsberg MH, Plow EF, Ruoslahti E. Platelet membrane glycoprotein IIb/IIIa: Member of a family of Arg-Gly-Asp-specific adhesion receptors. *Science.* 1986;231(4745):1559–62.
- Ruoslahti E, Pierschbacher MD. New perspectives in cell adhesion: RGD and integrins. *Science.* 1997;238(4826):491–7.
- Hersel U, Dahmen C, Kessler H. RGD modified polymers: biomaterials for stimulated cell adhesion and beyond. *Biomaterials.* 2003;24(24):4385–415.
- Bellis SL. Advantages of RGD peptides for directing cell association with biomaterials. *Biomaterials.* 2011;32(18):4205–10.
- Hansson A, Hashom N, Falson F, Rousselle P, Jordan O, Borchard G. *In vitro* evaluation of an RGD-functionalized chitosan derivative for enhanced cell adhesion. *Carbohydr Polym.* 2012;90(4):1494–500.
- Shin YC, Lee JH, Jin L, Kim MJ, Kim C, Hong SW, et al. Cell-adhesive matrices composed of RGD peptide-displaying M13 bacteriophage/poly(lactide-co-glycolic acid) nanofibers beneficial to myoblast differentiation. *J Nanosci Nanotechnol.* 2015;15:7907–12.
- Zhang Y, Nayak TR, Hong H, Cai W. Graphene: a versatile nanoplatform for biomedical applications. *Nanoscale.* 2012;4(13):3833–42.
- Chung C, Kim YK, Shin D, Ryoo SR, Hong BH, Min DH. Biomedical applications of graphene and graphene oxide. *Acc Chem Res.* 2013;46(10):2211–24.
- Artiles MS, Rout CS, Fisher TS. Graphene-based hybrid materials and devices for biosensing. *Adv Drug Deliv Rev.* 2011;63(14–15):1352–60.
- Ding X, Liu H, Fan Y. Graphene-based materials in regenerative medicine. *Adv Healthc Mater.* 2015;4(10):1451–68.
- Ku SH, Park CB. Myoblast differentiation on graphene oxide. *Biomaterials.* 2013;34(8):2017–23.
- Bajaj P, Rivera JA, Marchwiany D, Solovyeva V, Bashir R. Graphene-based patterning and differentiation of C2C12 myoblasts. *Adv Healthc Mater.* 2014;3(7):995–1000.
- Chaudhuri B, Bhadra D, Moroni L, Pramanik K. Myoblast differentiation of human mesenchymal stem cells on graphene oxide and electrospun graphene oxide-polymer composite fibrous meshes: importance of graphene oxide conductivity and dielectric constant on their biocompatibility. *Biofabrication.* 2015;7(1):015009.
- Lee EJ, Lee JH, Jin L, Jin OS, Shin YC, Sang JO, et al. Hyaluronic acid/poly(lactide-co-glycolic acid) core/shell fiber meshes loaded with epigallocatechin-3-O-gallate as skin tissue engineering scaffolds. *J Nanosci Nanotechnol.* 2014;14(11):8458–63.
- Dalton PD, Vaquette C, Farrugia BL, Dargaville TR, Brown TD, Hutmacher DW. Electrospinning and additive manufacturing: converging technologies. *Biomater Sci.* 2013;1(2):171–85.
- Pan Z, Ding J. Poly(lactide-co-glycolide) porous scaffolds for tissue engineering and regenerative medicine. *Interface Focus.* 2012;2(3):366–77.
- Mo Y, Guo R, Liu J, Lan Y, Zhang Y, Xue W, et al. Preparation and properties of PLGA nanofiber membranes reinforced with cellulose nanocrystals. *Colloids Surf B Biointerfaces.* 2015;132:177–84.
- Chia HN, Wu BM. Recent advances in 3D printing of biomaterials. *J Biol Eng.* 2015;9:4.
- Lee SW, Belcher AM. Virus-based fabrication of micro- and nanofibers using electrospinning. *Nano Lett.* 2004;4(3):387–90.
- Wang J, Wang L, Li X, Mao C. Virus activated artificial ECM induces the osteoblastic differentiation of mesenchymal stem cells without osteogenic supplements. *Sci Rep.* 2013;3:1242–8.
- Merzlyak A, Indrakanti S, Lee SW. Genetically engineered nanofiber-like viruses for tissue regenerating materials. *Nano Lett.* 2009;9(2):846–52.
- Yoo SY, Kobayashi M, Lee PP, Lee SW. Early osteogenic differentiation of mouse preosteoblasts induced by collagen-derived DGEA-peptide on nanofibrous phage tissue matrices. *Biomacromolecules.* 2011;12(4):987–96.
- Lee BY, Zhang J, Zueger C, Chung WJ, Yoo SY, Wang E, et al. Virus-based piezoelectric energy generation. *Nat Nanotechnol.* 2012;7(6):351–6.
- Liu F, Guo R, Shen M, Wang S, Shi X. Effect of processing variables on the morphology of electrospun poly[(lactide acid)-co-(glycolic acid)] nanofibers. *Macromol Mater Eng.* 2009;294(10):666–72.
- Deitzel JM, Kleinmeyer J, Harris D, Tan NCB. The effect of processing variables on the morphology of electrospun nanofibers and textiles. *Polymer.* 2001;42(1):261–72.
- Wang Z, Zhao Y, Luo Y, Wang S, Shen M, Tomás H, et al. Attapulgite-doped electrospun poly(lactide-co-glycolic acid) nanofibers enable enhanced osteogenic differentiation of human mesenchymal stem cells. *RSC Adv.* 2015;5(4):2383–91.
- Ryu YJ, Kim HY, Lee KH, Park HC, Lee DR. Transport properties of electrospun nylon 6 nonwoven mats. *Eur Polym J.* 2003;39(9):1883–9.
- Pham QP, Sharma U, Mikos AG. Electrospinning of polymeric nanofibers for tissue engineering applications: A review. *Tissue Eng.* 2006;12(5):1197–211.
- Sabba D, Mathews N, Chua J, Pramana SS, Mulmudi HK, Wang Q, et al. High-surface-area, interconnected, nanofibrillar TiO₂ structures as photoanodes in dye-sensitized solar cells. *Scripta Mater.* 2013;68(7):487–90.
- Khalil KA, Fouad H, Elsarnagawy T, Almajhdi FN. Preparation and characterization of electrospun PLGA/silver composite nanofibers for biomedical applications. *Int J Electrochem Sci.* 2013;8:3483–93.

41. Meng ZX, Wang YS, Ma C, Zheng W, Li L, Zheng YF. Electrospinning of PLGA/gelatin randomly-oriented and aligned nanofibers as potential scaffold in tissue engineering. *Mat Sci Eng C*. 2010;30(8):1204–10.
42. Jackson M, Choo LP, Watson PH, Halliday WC, Mantsch HH. Beware of connective tissue proteins: assignment and implications of collagen absorptions in infrared spectra of human tissues. *Biochim Biophys Acta*. 1995;1270(1):1–6.
43. Sionkowska A, Wisniewski M, Skopinska J, Kennedy CJ, Wess TJ. Molecular interactions in collagen and chitosan blends. *Biomaterials*. 2004;25(5):795–801.
44. Hernández B, Pflüger F, Nsangou M, Ghomi M. Vibrational analysis of amino acids and short peptides in hydrated media. IV. Amino acids with hydrophobic side chains: L-alanine, L-valine, and L-isoleucine. *J Phys Chem B*. 2009;113(10):3169–78.
45. Maiti NC, Apetri MM, Zagorski MG, Carey PR, Anderson VE. Raman spectroscopic characterization of secondary structure in natively unfolded proteins: α -synuclein. *J Am Chem Soc*. 2004;126(8):2399–408.
46. O'Brien DP, Hernandez B, Durand D, Hourdel V, Sotomayor-Pérez AC, Vachette P, et al. Structural models of intrinsically disordered and calcium-bound folded states of a protein adapted for secretion. *Sci Rep*. 2015;5:14223.
47. Zanni E, De Bellis G, Bracciale MP, Broggi A, Santarelli ML, Sarto MS, et al. Graphite nanoplatelets and *Caenorhabditis elegans*: Insights from an *in vivo* model. *Nano Lett*. 2012;12(6):2740–4.
48. Lv M, Zhang Y, Liang L, Wei M, Hu W, Li X, et al. Effect of graphene oxide on undifferentiated and retinoic acid-differentiated SH-SY5Y cells line. *Nanoscale*. 2012;4(13):3861–6.
49. Chang Y, Yang ST, Liu JH, Dong E, Wang Y, Cao A, et al. *In vitro* toxicity evaluation of graphene oxide on A549 cells. *Toxicol Lett*. 2011;200(3):201–10.
50. Ruiz ON, Fernando KA, Wang B, Brown NA, Luo PG, McNamara ND, et al. Graphene oxide: A nonspecific enhancer of cellular growth. *ACS Nano*. 2011;5(10):8100–7.
51. Olson EN. Interplay between proliferation and differentiation within the myogenic lineage. *Dev Biol*. 1992;154(2):261–72.
52. Redfield A, Nieman MT, Knudsen KA. Cadherins promote skeletal muscle differentiation in three-dimensional cultures. *J Cell Biol*. 1997;138(6):1323–31.
53. Swailes NT, Colegrave M, Knight PJ, Peckham M. Non-muscle myosins 2A and 2B drive changes in cell morphology that occur as myoblasts align and fuse. *J Cell Sci*. 2006;119(17):3561–70.
54. Musa H, Orton C, Morrison EE, Peckham M. Microtubule assembly in cultured myoblasts and myotubes following nocodazole induced microtubule depolymerisation. *J Muscle Res Cell M*. 2003;24(4–6):301–8.
55. Amack JD, Mahadevan MS. The myotonic dystrophy expanded CUG repeat tract is necessary but not sufficient to disrupt C2C12 myoblast differentiation. *Hum Mol Genet*. 2001;10(18):1879–87.
56. Bajaj P, Reddy Jr B, Millet L, Wei C, Zorlutuna P, Bao G, et al. Patterning the differentiation of C2C12 skeletal myoblasts. *Integr Biol*. 2011;3(9):897–909.
57. Kitzmann M, Carnac G, Vandromme M, Primig M, Lamb NJ, Fernandez A. The muscle regulatory factors MyoD and Myf-5 undergo distinct cell cycle-specific expression in muscle cells. *J Cell Biol*. 1998;142(6):1447–59.
58. Kato K, Gurdon JB. Single-cell transplantation determines the time when *Xenopus* muscle precursor cells acquire a capacity for autonomous differentiation. *Proc Natl Acad Sci U S A*. 1993;90(4):1310–4.
59. Buckingham M. How the community effect orchestrates muscle differentiation. *Bioessays*. 2012;25(1):13–6.
60. Skerjanc IS, Slack RS, McBurney MW. Cellular aggregation enhances MyoD-directed skeletal myogenesis in embryonal carcinoma cells. *Mol Cell Biol*. 1994;14(12):8451–9.
61. Shin YC, Lee JH, Jin L, Kim MJ, Kim YJ, Hyun JK, et al. Stimulated myoblast differentiation on graphene oxide-impregnated PLGA-collagen hybrid fibre matrices. *J Nanobiotechnol*. 2015;13(1):21.
62. Chen GY, Pang DW, Hwang SM, Tuan HY, Hu YC. A graphene-based platform for induced pluripotent stem cells culture and differentiation. *Biomaterials*. 2012;33(2):418–27.
63. Park SY, Park J, Sim SH, Sung MG, Kim KS, Hong BH, et al. Enhanced differentiation of human neural stem cells into neurons on graphene. *Adv Mater*. 2011;23(36):H263–7.
64. Oh JW, Chung WJ, Heo K, Jin HE, Lee BY, Wang E, et al. Biomimetic virus-based colourimetric sensors. *Nat Commun*. 2014;5:3043.
65. Hummers WS, Offeman RE. Preparation of graphitic oxide. *J Am Chem Soc*. 1958;80(6):1339.
66. Shin YC, Lee JH, Jin OS, Kang SH, Hong SW, Kim B, et al. Synergistic effects of reduced graphene oxide and hydroxyapatite on osteogenic differentiation of MC3T3-E1 preosteoblasts. *Carbon*. 2015;95:1051–60.
67. Lee JH, Shin YC, Jin OS, Lee EJ, Han DW, Kang SH. Cytotoxicity evaluations of pristine graphene and carbon nanotubes in fibroblastic cells. *J Korean Phys Soc*. 2012;61(6):873–7.
68. Majewska A, Yiu G, Yuste R. A custom-made two-photon microscope and deconvolution system. *Pflug Arch Eur J Phys*. 2000;441(2–3):398–408.
69. Hovhannisyanyan V, Hu PS, Chen SJ, Kim CS, Dong CY. Elucidation of the mechanisms of optical clearing in collagen tissue with multiphoton imaging. *J Biomed Opt*. 2013;18(4):046004.

Submit your next manuscript to BioMed Central and we will help you at every step:

- We accept pre-submission inquiries
- Our selector tool helps you to find the most relevant journal
- We provide round the clock customer support
- Convenient online submission
- Thorough peer review
- Inclusion in PubMed and all major indexing services
- Maximum visibility for your research

Submit your manuscript at
www.biomedcentral.com/submit

